

# Interplay of Kelvin–Helmholtz and superradiant instabilities of an array of quantized vortices in a two-dimensional Bose–Einstein condensate

Luca Giacomelli\* and Iacopo Carusotto†  
*INO-CNR BEC Center and Dipartimento di Fisica,  
 Università di Trento, via Sommarive 14, I-38050 Povo, Trento, Italy*

We investigate the various physical mechanisms that underlie the dynamical instability of a quantized vortex array at the interface between two counter-propagating superflows in a two-dimensional Bose–Einstein condensate. Instabilities of markedly different nature are found to dominate in different flow velocity regimes. For moderate velocities where the two flows are subsonic, the vortex lattice displays a quantized version of the hydrodynamic Kelvin–Helmholtz instability (KHI), with the vortices rolling up and co-rotating. For supersonic flow velocities, the oscillation involved in the KHI can resonantly couple to acoustic excitations propagating away in the bulk fluid on both sides. This makes the KHI rate to be effectively suppressed and other mechanisms to dominate: For finite and relatively small systems along the transverse direction, the instability involves a repeated superradiant scattering of sound waves off the vortex lattice; for transversally unbound systems, a radiative instability dominates, leading to the simultaneous growth of a localized wave along the vortex lattice and of acoustic excitations propagating away in the bulk. Finally, for slow velocities, where the KHI rate is intrinsically slow, another instability associated to the rigid lateral displacement of the vortex lattice due to the vicinity of the system’s boundary is found to dominate.

## I. INTRODUCTION

Parallel flows in hydrodynamics are known to give rise to instabilities, one of the most fundamental ones being the Kelvin–Helmholtz instability (KHI) occurring in the *shear layer* separating two parallel uniform flows [1]. The effect of this instability is to amplify perturbations located in the transition region and create a characteristic vortex-like flow pattern that grows until the two flows mix up in a turbulent way.

The KHI is an inviscid phenomenon, determined by inertial effects and not by viscosity; as such, it can be expected to also take place in the inviscid flow of superfluids. In this context, KHI was experimentally observed at the interface between the two superfluid phases of  $^3\text{He}$  [2, 3]. More recently, dilute Bose–Einstein condensates (BECs) of ultracold atoms have been considered for the study of this phenomenon: in particular, KHI was shown to develop in phase-separated two-component BECs [4, 5], while the KHI of a quantized vortex array in a single component condensate was explored in [6]. Given the irrotational nature of the velocity field of a single-component BEC, the only way to accommodate the velocity difference is in fact by creating an array of quantized vortices along the shear layer. In this work, the vortex array is formed by progressively lowering a potential barrier between the two counterpropagating flows. In the subsequent evolution, the vortices are then found to roll up and clusterize, with a behaviour closely analogous to the one of the classical shear layer.

The KHI occurs in incompressible fluids both in the case of a sharp vortex sheet (or tangential discontinuities, §29 in [7]) and in the case of smooth transition

between the two uniform parallel flows. Here, the effect of the finite width of the shear layer is to quench the instability at smaller scales [1]. New features are found when compressible fluids are considered, in particular for relative velocities  $\Delta v$  of the order of twice the speed of sound in the fluid. For a vortex sheet in two spatial dimensions the KHI is suppressed and the discontinuity becomes stable again for  $\Delta v > 2\sqrt{2}c_s$  (see Problem 1 in §84 of [7]). In the case of a finite-size shear layer, the instability is present for all values of  $\Delta v$ , but displays different properties for  $\Delta v > 2c_s$  (see for example [8] for complete references).

This change in behaviour is due to the wave-like character of acoustic perturbations in compressible fluids, that display a negative energy in supersonic flows. This same feature also underlies the amplified reflection (or over-reflection) of acoustic waves at an interface with  $\Delta v > 2c_s$  (Problem 2 in §84 of [7]). Within the gravitational analogy framework [9], this phenomenon can be related to superradiant scattering from rotating black holes [10], whose analog has been recently observed in a water tank displaying a draining vortex flow configuration [11]. In parallel flows instead, amplified reflection is typically associated to dynamical instabilities that complicate the picture (see for example discussion in §11.5 of [12]).

In this article we investigate the interplay of superradiant phenomena and the KHI of an array of quantized vortices in an atomic BEC like the one considered in [6]. While the standard KHI is recovered for  $\Delta v < 2c_s$ , a much richer physics is found for  $\Delta v > 2c_s$  when the KHI can mix with propagating sound waves and gets effectively quenched. In finite-size configurations along the direction transverse to the velocity, the KHI is replaced by a slower instability: the perturbation starts to appear in the bulk of the two counterpropagating flows and only at later times it produces a significant distortion of

\* luca.giacomelli-1@unitn.it

† iacopo.carusotto@unitn.it

the vortex array. This superradiant instability (SRI) can be understood in terms of a repeated amplified scattering of sound waves in the two surrounding bulk regions, that are then bounced back towards the interface by the edges of the system. A related superradiant instability was studied in [13] in a configuration where the velocity jump was created by a static synthetic gauge field with no independent dynamics.

Moreover, while this seems to suggest that the parallel flow should be stable in an unbound system (when the effect of repeated amplifications is removed), surprisingly we find that the system displays another kind of instability in which a *surface mode* localized in the shear layer grows together with acoustic modes propagating away in the two flows. This *radiative instability* (RI) is analogous to the ergoregion instabilities of multiply quantized vortices that we studied in [14].

While in the KHI and the SRI regimes the long-distance hydrodynamic picture captures the essential physics, in the RI regime the short-distance quantized nature of the shear layer becomes important for the existence of localized excitations that are resonant with travelling ones. This quantization becomes also important when small velocities are considered, for which we find that the dominating instability is associated to a rigid lateral displacement of the vortices. This drifting increases its velocity when the system size is decreased and is analogous to the precession of off-center vortices in cylindrically-symmetric trapped condensates [15]. This however does not prevent the development of the KHI that continues to dominate the long-time evolution of the system.

In the following we attack the problem by numerically studying the time evolution of the Gross-Pitaevskii equation (GPE) and by solving the linearized Bogoliubov problem on top of the *quantized vortex sheet* configuration with a Bloch-waves approach.

The structure of the paper is as follows. In Section II we introduce the system under study and show the results of GPE numerical calculations that display two different kinds of instability. In Section III we approach the problem by computing the Bloch-waves Bogoliubov spectra at different velocities. In the Section IV we describe in detail the different instability regimes: in Section IV A we describe the KHI regime, in Section IV B we discuss the SRI and RI, and in Section IV C we address what happens at small velocities. Finally, in Section V we draw the conclusions.

## II. GPE SIMULATIONS

We consider an atomic BEC at  $T = 0$  in a *pancake* shape, that is tightly confined in one direction so that the relevant dynamics takes place in two spatial dimensions. The condensate can be described with the GPE for the classical complex field in two spatial dimensions  $\Psi(t, x, y)$ , that is the order parameter of the BEC phase

transition [16]:

$$i\hbar\partial_t\Psi = \left[ -\frac{\hbar^2\nabla^2}{2M} + g|\Psi|^2 + V_{\text{ext}}(t, y) \right] \Psi. \quad (1)$$

Here  $M$  is the atomic mass,  $g$  is the interatomic interaction constant and  $V_{\text{ext}}$  is an external potential that, as indicated, we take to depend only on  $y$  and possibly time-dependent. The order parameter of a stationary state of the GPE can be taken in the shape  $\Psi(t, x, y) = e^{-i\mu t/\hbar} \sqrt{n(t, x, y)} e^{i\Theta(t, x, y)}$ , where  $\mu$  is the chemical potential,  $n$  is the density of condensed atoms and  $\Theta$  is the phase, that is related to the velocity of the condensate by  $\mathbf{v} = \hbar\nabla\Theta/M$ . Interactions imply the presence of a finite sound speed, that in a constant-density condensate is  $c_s := \sqrt{gn/M}$ , and introduce a typical length scale, the so-called *healing length*  $\xi := \hbar/Mc_s$ .

As was done in [6], we consider periodic boundary conditions along  $x$  and a potential composed by two hard walls at  $y = \pm L_y/2$  and by a repulsive Gaussian potential centered in  $y = 0$ . The Gaussian potential is initially strong enough so that the condensate is composed by two parts separated and independent, as shown in the leftmost panels of Figure 1. The ground state of the GPE with this potential is computed via imaginary-time propagation and at  $t = 0$  the two condensates are given equal and opposite *momentum kicks*, so that they develop equal and opposite velocities  $\pm v = \pm\Delta v/2$  along  $x$ . The intensity of the central Gaussian potential is then linearly decreased in time so to vanish at  $t = 100 \mu\hbar$ , after which the external potential is composed only by the time-independent hard walls. After the central barrier is lowered the only way for the condensate to satisfy the irrotationality of the velocity vector field is to create an array of (singly) quantized vortices along  $y = 0$ , in numbers equal to the difference of the winding numbers of the phase in the two channels. In other words, given a relative velocity  $\Delta v$  between the two condensates, the number of vortices per unit length will be

$$n_{\text{vort}} = \frac{M}{\hbar} \frac{\Delta v}{2\pi}. \quad (2)$$

For values of  $x$  that do not correspond to a vortex, the  $y$  dependence of the transverse velocity  $v_x$  can in good approximation be fitted with a functional form of the shape  $v_x(y) = v \tanh(y/\delta_v)$ , with  $\delta_v$  width of the transition region between the two counterpropagating uniform flows  $\pm v$ . This is a well-known velocity profile in hydrodynamics, whose KHI for an incompressible fluid was studied in [17], and whose stability in the case of a compressible fluid was characterized in [18]. Fits of the numerical data obtained from the GPE show that, while increasing the velocity, the width of the shear layer decreases approximately as

$$\delta_v \simeq \frac{\hbar}{M} \frac{1}{2v}. \quad (3)$$

In Figure 1 we show, for two different relative velocities, snapshots of the time-evolution of the GPE following this procedure. In the first example, for  $\Delta v < 2c_s$ ,

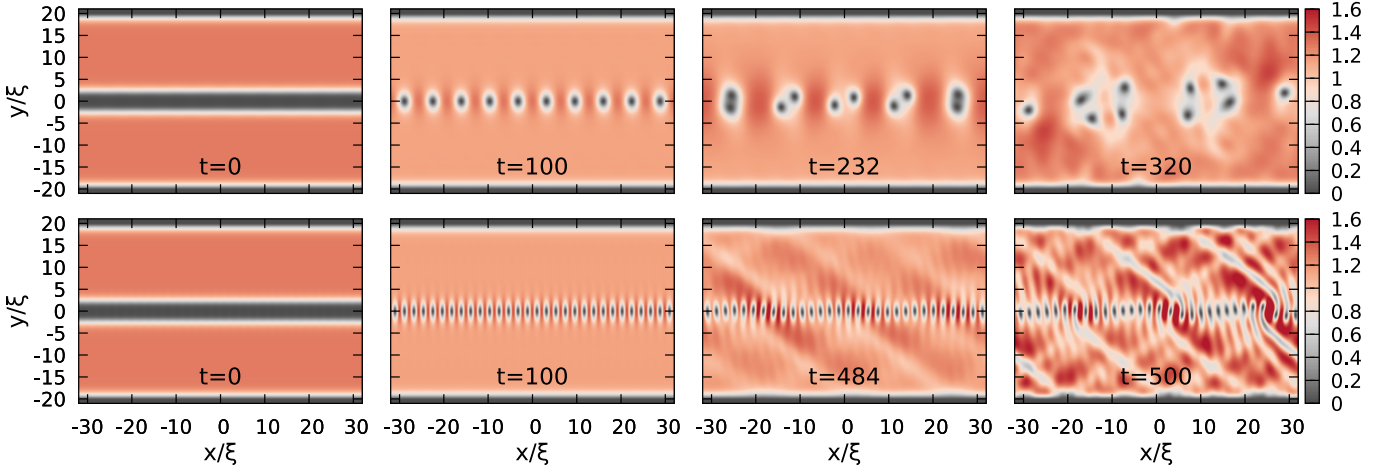


FIG. 1. Time evolutions (obtained by solving the GPE (1)) of the density of a condensate confined along  $y$  by hard walls and with a central Gaussian potential  $V_G = A \exp(-y^2/2\sigma^2)$  with  $A = 5\mu$  and  $\sigma = \xi$ . Opposite velocities are imposed for the two parts of the system and, when the Gaussian potential is progressively lowered (between  $t = 0$  and  $t = 100 \mu/\hbar$ ), an array of quantized vortices develops. The upper plots show the case  $\Delta v = 0.98 c_s$  and the lower ones  $\Delta v = 2.94 c_s$ . The first case shows the KHI behaviour presented in [6], in which vortices clusterize and co-rotate. The second one is an example of SRI, in which the instability is slower and the unstable mode is not localized on the vortex line, but spreads all over the system. Times are expressed in units of  $\hbar/\mu$ .

the vortex line is unstable with a mechanism similar to the hydrodynamic KHI: after some time vortices start to move from the horizontal  $y = 0$  line and begin to co-rotate in clusters of growing size, that were characterized in [6]. In the second example instead, in which  $\Delta v > 2c_s$ , even if the vortices are much closer, they do not move initially from the horizontal line and an unstable growing mode develops in the whole system, as can be seen from the emerging pattern. Surprisingly, the vortices take a longer time to move and do so together with significant density variations in the *bulk* of the two flows. The emerging pattern in this second case indicates that the instability is due to a superposition of up-going and down-going waves, and hence that phononic propagating modes are involved.

Further evidence on the difference of localization of the unstable modes in the two cases is obtained by varying the vertical size of the system  $L_y$ , that is the separation between the two hard walls. We observe that for  $\Delta v < 2c_s$  the time for the vortex line to deform is essentially independent from  $L_y$ , while for  $\Delta v > 2c_s$  the instability rate decreases while increasing  $L_y$ . All these features suggest that the origin of the second kind of instability is the same of the superradiant instabilities (SRI) we observed in [13], in which propagating modes of opposite energies are involved, giving rise to the same kind of pattern. Also, the  $\Delta v > 2c_s$  threshold for this kind of instability is the same in the two cases.

While strikingly showing the different instability mechanisms, time evolutions of the GPE are not the best tool to obtain a complete picture of the phenomenon. The long time the instability takes to significantly deform the line of vortices indicates that the configuration obtained when the central Gaussian potential is lowered

is a stationary state  $\Psi_v(x, y)$  of the GPE. This is confirmed by the fact that imaginary time evolutions of the GPE with fixed winding numbers in the two channels converge to states of the shape we found with the above time-dependent procedure. In the following we hence resort to a study of the linear stability of this stationary state with a Bogoliubov approach.

### III. BLOCH FUNCTIONS FOR THE BOGOLIUBOV PROBLEM

The natural approach to the study of the Bogoliubov problem in this configuration is to take advantage of the periodic structure of the stationary states we are interested in; the vortices along  $y = 0$  are in fact equispaced along  $x$ , as can be seen in the second ( $t = 100$ ) panels of Figure 1. We consider a small deviation

$$\Psi(t, x, y) = e^{-i\mu t/\hbar} (\Psi_v(x, y) + \delta\psi(t, x, y)), \quad (4)$$

where the stationary state  $\Psi_v$  relative to a given velocity  $v$  in each channel has the periodicity

$$\Psi_v \left( x + \frac{2}{n_{\text{vort}}}, y \right) = \Psi_v(x, y). \quad (5)$$

While the periodicity of the complex order parameter  $\Psi_v$  is  $2/n_{\text{vort}}$ , what matter for fluctuations are the density and the velocity, that instead have a period  $1/n_{\text{vort}}$ . This can also be seen by the fact that in the linear problem (7) we are now going to write only the square of the order parameter enters.

The perturbations (4) around a stationary state are described at the linear level by the Bogoliubov equations,

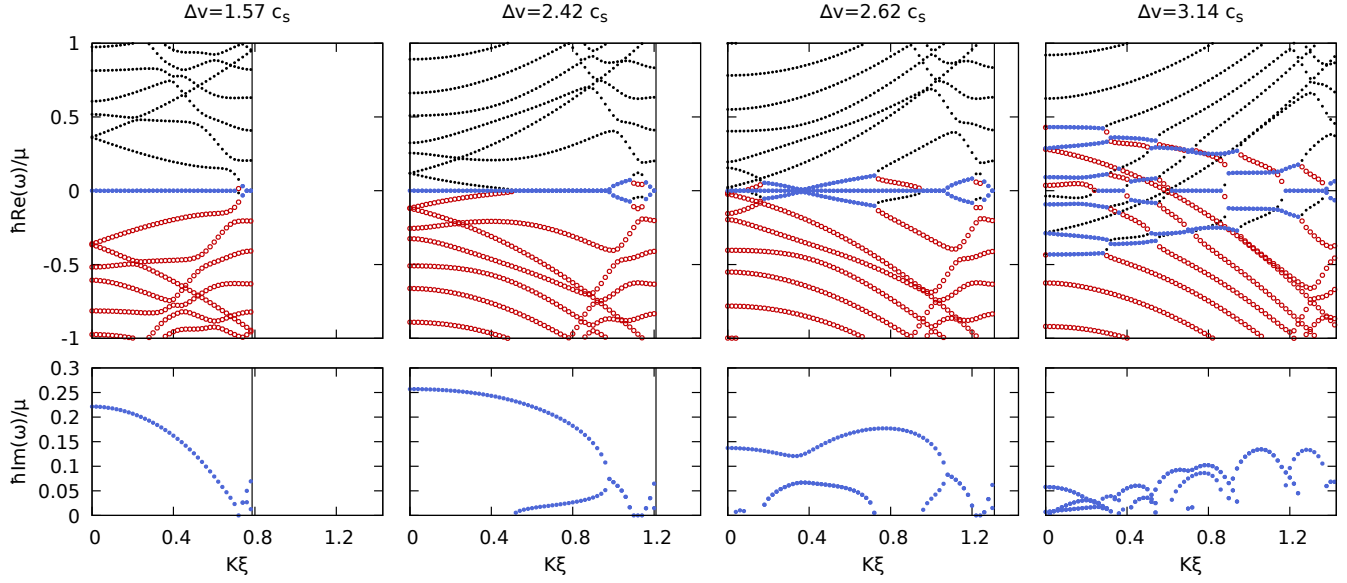


FIG. 2. Real (top panels) and imaginary (bottom panels) parts of the eigenfrequencies of the Bogoliubov problem for varying Bloch momentum  $K$  for vertical size  $L_y = 20\xi$  and for four different values of the relative velocity  $\Delta v$  in each parallel flow. The  $K$  range is truncated at the edge of each Brillouin zone. Black filled dots correspond to positive-norm modes, red empty dots to negative-norm ones and blue thicker dots to zero-norm dynamically unstable modes, giving rise to the *bubbles* of instability visible in the lower plots. At the crossing of the  $\Delta v = 2c_s$  threshold, energetic instabilities begin to be present. One can see the transition between a regime in which the zero-frequency KHI dominates to a regime of SRI, in which the instability maxima occur at finite  $K$ .

that can be written, by considering  $\delta\psi$  and  $\delta\psi^*$  as independent variables [19], in terms of the Bogoliubov spinor

$$\begin{pmatrix} \delta\psi \\ \delta\psi^* \end{pmatrix}(x, y) = e^{iKx} \begin{pmatrix} U_K \\ V_K \end{pmatrix}(x, y), \quad (6)$$

that we decompose in decoupled Bloch waves, where  $U_K$  and  $V_K$  have the periodicity  $1/n_{\text{vort}}$  we just discussed, and  $K$  belongs to the first Brillouin zone  $-\frac{M}{\hbar}v \leq K \leq \frac{M}{\hbar}v$ . The resulting Bogoliubov equations at fixed  $v$  and  $K$  are

$$i\hbar\partial_t \begin{pmatrix} U_K \\ V_K \end{pmatrix} = \begin{bmatrix} D_{v,K} & g\Psi_v^2 \\ -g(\Psi_v^*)^2 & -D_{v,K} \end{bmatrix} \begin{pmatrix} U_K \\ V_K \end{pmatrix} =: \mathcal{L}_{v,K} |\phi_K\rangle, \quad (7)$$

with

$$D = -\frac{\hbar^2\nabla^2}{2M} - \frac{i\hbar K}{M}\partial_x + \frac{\hbar^2K^2}{2M} + 2g|\Psi_v|^2 + V_{\text{ext}} - \mu. \quad (8)$$

The matrix involved in the Bogoliubov equations is not Hermitian, however it is  $\sigma_3$ -pseudo-hermitian, that is  $\sigma_3\mathcal{L}_{v,K}^\dagger\sigma_3 = \mathcal{L}_{v,K}$ . This implies that the evolution through the Bogoliubov equations conserves energy, but the energy of an eigenmode  $|\phi_{K,i}\rangle$  of  $\mathcal{L}_{v,K}$  is not given simply by its frequency, but by

$$E_{K,i} = \|\phi_{K,i}\|_B \hbar\omega_{K,i}, \quad (9)$$

where  $\|\phi_{K,i}\|_B := \int dx dy (|U_K|^2 - |V_K|^2)$  is the so-called Bogoliubov norm of the eigenmode. This can have both

signs (and also be zero), so that for example negative-norm modes at positive frequencies have a negative energy; the presence of negative-energy modes is referred to as *energetic instability*. Zero-norm modes are instead associated to complex eigenvalues, that come in pairs of complex-conjugate frequencies; the modes with positive imaginary part of the frequencies are exponentially growing and are known as *dynamical instabilities*. These have zero energy and can emerge with the resonance of two opposite-normed modes, so that they can be thought as the simultaneous production of excitations with opposite energies.

To solve the Bogoliubov problem we compute, for a fixed  $v$ , the order parameter with an imaginary-time propagation of the GPE on a numerical  $x$  range of  $2/n_{\text{vort}}$ , imposing unit winding number in each channel, and we then construct the Bogoliubov matrix with half of the  $x$  range of the obtained  $\Psi_v$  and using discretized expressions for the derivatives. We diagonalize this matrix, for a given Bloch momentum  $K$ , and repeat the diagonalization sampling all the  $K$ -s in the first Brillouin zone for the given  $v$ . Examples of the obtained spectra for different values of the velocity of the two opposite parallel flows are shown in Figure 2.

One can see that for  $\Delta v < 2c_s$  the spectra are composed of positive-energy modes (positive-norm at positive frequencies and negative-norm at negative ones) and by a dynamically unstable branch with zero real part of the frequency, whose instability rate increases while ap-

proaching  $K = 0$ . As we are going to discuss, these are the unstable modes responsible for the KHI. For  $\Delta v > 2c_s$  instead the positive- and negative-norm parts of the spectra merge, reflecting the energetic instability associated to the Landau instability of supersonic flows in both the upper and the lower part of the system. As we already anticipated, the pseudo-Hermitian nature of the Bogoliubov problem implies that when modes of opposite norm sign approach, they give rise to a dynamically unstable branch.

The closing of the gap between the positive- and negative-norm modes for all the Bloch momenta perturbs the zero-frequency KHI branch, suppressing it. For high enough velocities in fact the KHI behaviour dominated by small Bloch momenta is replaced by (lower) maxima at finite  $K$ . The physical meaning of this behaviour of the spectra is that the modes responsible for the KHI couple to collective modes of the two channels when these are resonant, so that the KHI is effectively *damped* by the emission of phonons in the two parallel flows. The physics is hence dominated by different effects, that we are going to discuss in the following.

A quick picture of the instability regimes can be obtained by looking at Figure 3 in which we show, for three different  $L_y$ , the maximum instability rate for different values of  $v$  and the corresponding Bloch momentum. Besides the two regimes already observed from the GPE calculation, a third behaviour is visible at small velocities  $\Delta v \lesssim 0.8c_s$ , for which the maximum instability rate occurs for Bloch momenta at the edge of the Brillouin zone and does not strongly depend on the relative velocity. For intermediate velocities instead the maximum instability occurs for  $K = 0$ , increases linearly with the velocity and is independent on the system size; this is the KHI regime. For higher velocities  $\Delta v > 2c_s$  the maximum instability rate occurs for finite values of  $K$  (increasing with  $v$ ), approaches a constant for increasing velocities and strongly depends on the system size; this is the SRI regime. The fact that the transition from KHI to SRI does not occur abruptly at  $\Delta v = 2c_s$  is because of the finite vertical size of the system that results in a spacing between the available phononic modes in the two regions. One can see from the upper panel of Figure 3 that the width of the transition region is smaller for larger systems, so that one can expect the transition to occur exactly at  $\Delta v = 2c_s$  in an infinite system, in which a continuum of phononic modes is available.

In the next Section we consider in detail each of these regimes.

#### IV. INSTABILITY REGIMES

##### A. Moderate velocities: Kelvin–Helmholtz instability

In hydrodynamics the KHI for a (continuous) vortex sheet, i.e. a tangential discontinuity between two parallel

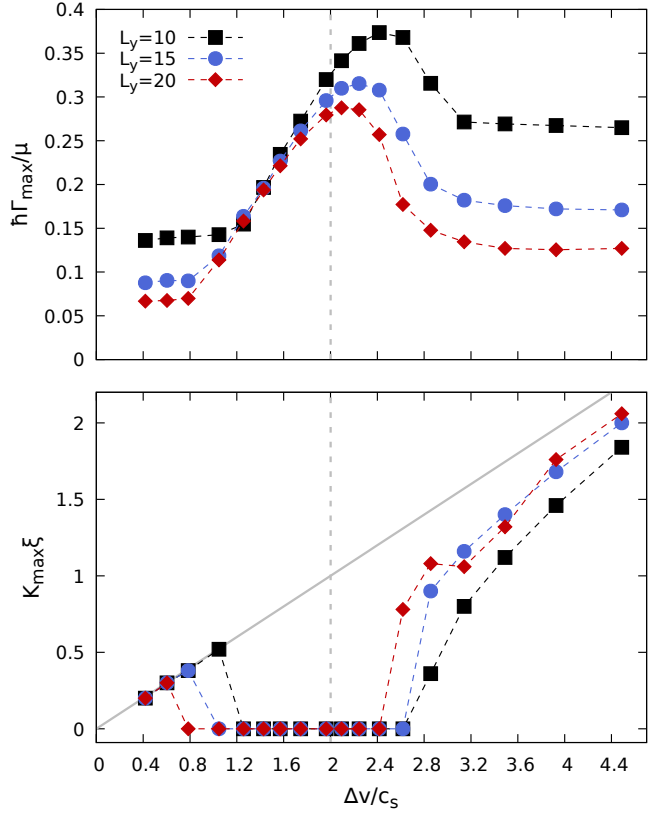


FIG. 3. Maxima (upper plot) and corresponding transverse momentum values (lower plot) of the instability rates for different values of  $\Delta v$ . Dashed lines are simply a guide for the eye, the solid gray line in the lower plot indicates the edge of the Brillouin zone and the vertical dashed gray lines indicate  $\Delta v = 2c_s$ . The three types of point correspond to different vertical sizes of the system  $L_y$ , as indicated in the legend of the upper plot.

flows  $v_1$  and  $v_2$ , is known to have the *dispersion relation* (see [1] Section 4.3.1)

$$\omega(k_T) = \frac{v_1 + v_2}{2} k_T \pm i \frac{v_1 - v_2}{2} k_T, \quad (10)$$

where  $k_T$  is the wavevector of the perturbation tangential to the discontinuity (parallel to the flows). This result is modified if, instead of a tangential discontinuity, a finite-width shear layer is present; for example for a continuous piecewise profile that is constant for  $|y| > \delta$  and changes linearly for  $-\delta \leq y \leq \delta$  the dispersion relation becomes (see [1] Section 4.3.2)

$$\omega = \frac{v_1 + v_2}{2} k_T \pm i \frac{v_1 - v_2}{4\delta} \sqrt{e^{-4k_T\delta} - (2k_T\delta - 1)^2}. \quad (11)$$

At low transverse momenta the instability rate increases linearly, as in the zero-thickness case (10), while at higher transverse momenta there is a decrease and above  $k_T\delta \sim 0.6$  the instability is quenched. An analogous suppression of the instability was found in [17] for an hyperbolic tangent velocity profile, that we said is similar to the one of our case.

We can compare this hydrodynamic prediction with the result of our Bogoliubov analysis. First of all notice that, since our case corresponds to  $v_1 = -v_2 = \Delta v/2$ , the fact that we found the KHI branch at zero real part of the frequency is in accordance with equation (11). Moreover, from the upper plot of Figure 3, we see that between  $\Delta v \sim 0.8 c_s$  and  $\Delta v \sim 1.6 c_s$  the maximum instability rate increases linearly with  $\Delta v$ , in agreement with the linear dependence on the velocity difference of the imaginary part of (11).

To compare the momentum dependence of the instability rate we need to take into account that, because of our choice of the shape of fluctuations (4), in which the spatial phase of the stationary state is not taken as an overall factor, our Bloch momentum  $K$  differs from the hydrodynamic transverse momentum  $k_T$ , that is instead measured with respect to the fluid. In particular, the hydrodynamic momentum  $k_T$  is the one of the field  $\phi$  in the expression  $\Psi(t, x, y) = e^{-i\mu t/\hbar} \Psi_v(x, y) (1 + \phi(t, x, y))$ ; the two momenta are hence related by  $k_T = K \pm Mv/\hbar$ . Also considered the symmetry of the spectrum under a change of sign of  $K$ , we have that, in the Brillouin zone we are considering, the relation between the two momenta is

$$K = \frac{M}{\hbar} v - k_T. \quad (12)$$

Hence the prediction we should compare with our results is the *specular* of equation (11), that is, while going from the edge of the Brillouin zone towards decreasing Bloch momenta, a linear increase of the instability rate that then *bends* because of the finite width of the vorticity layer. This is exactly what we observe in the lower plot of the first case in Figure 2. The suppression of the instability predicted in the hydrodynamic case is instead not observed here. This can be interpreted with the fact that the threshold for the suppression  $k_T \gtrsim 0.6/\delta$  is fixed by the width of the shear layer, that in our case is velocity-dependent and given by (3); according to that scaling  $0.6/\delta_v > (M/\hbar)v$ , so that the hydrodynamic suppression threshold lies outside of the Brillouin zone. This means that the quantized nature of our shear layer removes the high- $k_T$  behaviour of the hydrodynamic prediction.

Notice that, while the Bloch momentum  $K$  of the fluctuation field  $\delta\psi$  is the most natural one to consider in our approach,  $k_T$  is the one that determines the spatial behaviour of density fluctuations  $\delta n = 2\text{Re}(\Psi_v^* \delta\psi)$ . Hence the  $K = 0$  dominating instability in the KHI regime, corresponding to a fluctuation  $\delta\psi$  that (apart from the periodic part of the Bloch function) is constant throughout the system, corresponds to a density variation  $\delta n = 2\text{Re}(\Psi_v^* \delta\psi) \sim \cos(\frac{Mv}{\hbar} x)$ , that has correctly an opposite sign on neighboring vortices.

## B. High velocity: superradiant and radiative instability

As we already discussed, the transition from the KHI regime to the SRI one by increasing the flow velocity can

be seen in the last three plots of Figure 2, in which the emergence of energetic instabilities associated to the supersonic flows above  $\Delta v = 2c_s$  implies the existence of phononic modes with which the  $\text{Re}(\omega) = 0$  modes responsible for the KHI can couple, suppressing thus the instability. The presence of these negative energy modes signals the possibility to have superradiant scattering when these are resonant with a positive energy one; that is if a positive-energy wave impinges on the shear layer from one region and there is a resonant negative-energy mode in the other region, the positive-energy wave can be reflected with increased amplitude. Furthermore, if we consider a finite system along  $y$ , as in Figure 1, this scattering process will lead to a dynamical instability, since the reflection of the waves at the boundaries of the condensate will cause repeated amplification. This mechanism based on modes of opposite energies is the same giving rise to superradiant scattering and superradiant instabilities in rotating spacetimes and in gravitational analogues [10, 13].

This is the meaning of the dynamically unstable branches that occur when two eigenmodes of opposite norm sign (and hence opposite energy) approach the same frequency, as can be seen in the plots of the real part of the frequency of Figure 2. The result of this linear instability is the behaviour shown in the second row of Figure 1, the emerging pattern being due to the superposition of the up-going and down-going waves of opposite energies, whose transverse momentum is reflected in the maxima of the instability rate at finite values of  $K$  visible for example in the rightmost plot of Figure 2.

Notice that in hydrodynamic shear layers, in which the shear layer is translationally invariant along  $x$ , the  $\Delta v > 2c_s$  threshold for the onset of the SRI can be understood from the fact that for lower relative velocities a reference frame in which the flow is everywhere subsonic [13]. In the present discrete case instead the quantized vortices break the Galileian invariance along  $x$ , since there is a reference frame in which they do not move; superradiant phenomena can hence only occur when supersonic flows with respect to them are available, that is for  $\Delta v > 2c_s$ .

Given this picture, one expects the instability rate to depend on the *round-trip time* of excitations in the two regions, that is to decrease while increasing the vertical size of the system  $L_y$ . To verify this we computed the spectra analogously to what we did for Figure 2 but we fixed relative velocity and repeated the computation for different values of  $L_y$ . In Figure 4 we show the maximum instability rate for each size of the system. The black squares are the result for a velocity in the KHI regime, that as expected show little dependence on the system size; the red filled circles are instead the result for a velocity in the SRI regime. One can see that the instability rate decreases quickly with the system size, as expected, but for larger  $L_y$  approaches a finite value, and not zero as one would expect for a SRI.

To get a better picture of what happens to the SRI at larger sizes, in Figure 4 we also show the  $K$  correspond-

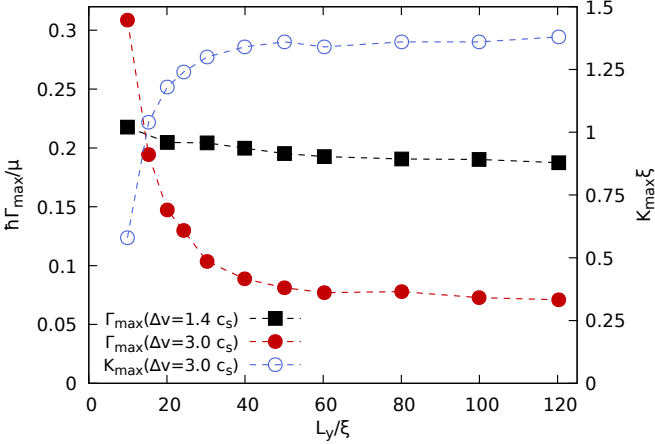


FIG. 4. Dependence of the instability maxima on the system size  $L_y$  for  $\Delta v = 1.4 c_s$  in the KHI regime (black squares) and for  $\Delta v = 3 c_s$  in the SRI/RI regime (filled red circles); empty blue circles show instead the location of the maximum in this second case ( $y$  axis on the right).

ing to the maximum instability rate (blue empty circles) and in the upper plots of Figure 5 we show the instability rates of all the dynamically unstable modes for four values of  $L_y$ . One can see that while  $L_y$  is increased the instability *bubbles* increase in number, corresponding to the increased density of modes in the larger system, that gives rise to more dynamically unstable branches. Moreover the height of these bubbles decreases in, as one would expect for a SRI. However, for large systems, a branch of unstable modes becomes visible, that depends little on the system size, as can be seen by comparing the  $L_y = 60\xi$  and the  $L_y = 120\xi$  plots in Figure 5. From this comparison one can expect instabilities in the infinite system at all  $K$ , while the maximum instability rate occurs in the rightmost bubble, near the edge of the Brillouin zone.

While the density of modes in the large systems becomes too high to make plots of the real part of the frequencies effective, in the lower panel of Figure 5 we show the main features of the spectrum in the infinite system, that can be inferred from the result for  $L_y = 120\xi$ . The red shaded region is where the Landau energetic instabilities associated to the supersonic motion are present. In finite systems these will give rise to dynamical instabilities, whose instability rates are the ones that can be seen in large number for example in the panel  $L_y = 120\xi$  of Figure 5 below the main unstable branch. In an infinite system instead the repeated amplifications at the basis of the SRI can not take place and only the energetic instabilities are left; these signal the possibility of superradiant scattering for phononic modes with frequencies in the red shaded region of the lower panel of Figure 5.

The blue line instead is the branch of modes that in the large finite system  $L_y = 120\xi$  have the largest instability rates at each  $K$ , and that are expected to remain dynamically unstable also in the infinite system. The part of the

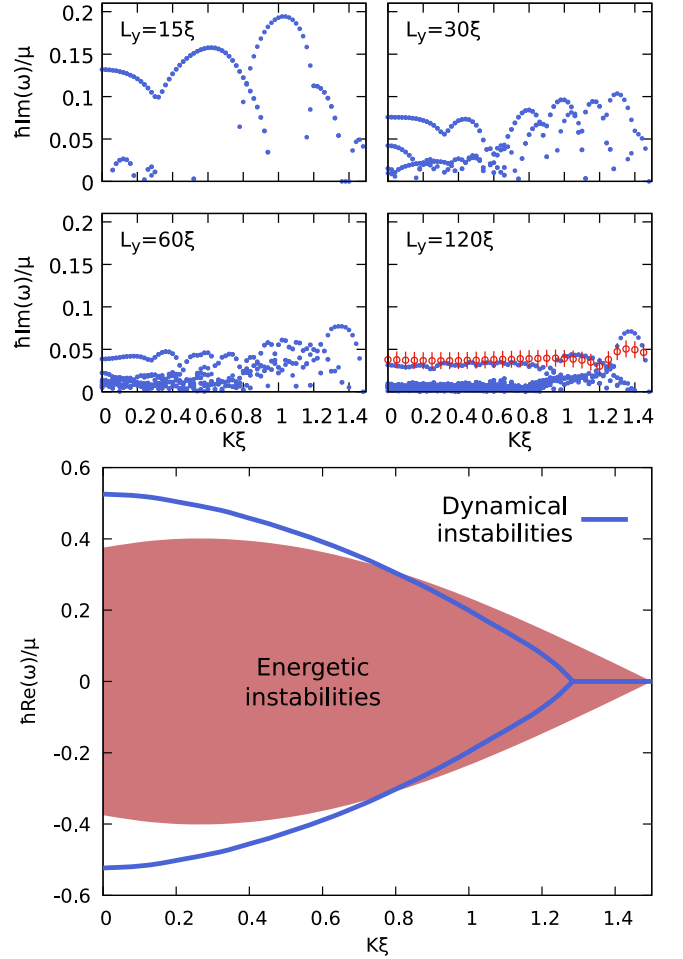


FIG. 5. Upper plots: instability rates of all the dynamically unstable modes for  $\Delta v = 3 c_s$  and four vertical system sizes. For  $L_y = 120\xi$  we also show with red empty circles the instability rates extracted from the time-dependent calculations of Figure 6. The error bars are given by the evolution time of our simulations. Lower plot: schematics of the real part of the spectrum in the infinite system. The red filled area is where the energetic instabilities associated to superradiant scattering are present, while in the white space around only positive-energy modes are present. The blue line is instead the dynamically unstable branch responsible for the RI.

spectrum at the edge of the Brillouin zone in which the branches at finite  $Re(\omega)$  join at  $Re(\omega) = 0$  corresponds to the highest bubble visible in the imaginary part of the spectrum.

The fact that this branch remains dynamically unstable in the infinite system can be confirmed by a time-dependent simulation of the Bogoliubov problem. We performed a time evolution of the two-dimensional Bogoliubov equations (7) for  $K = 0$  and on a background composed by many *lattice cells*, so to sample many Bloch momentum values together, and starting from a noisy configuration to seed instabilities. Regions of absorbing potential for the fluctuations are included near  $\pm L_y/2$  to

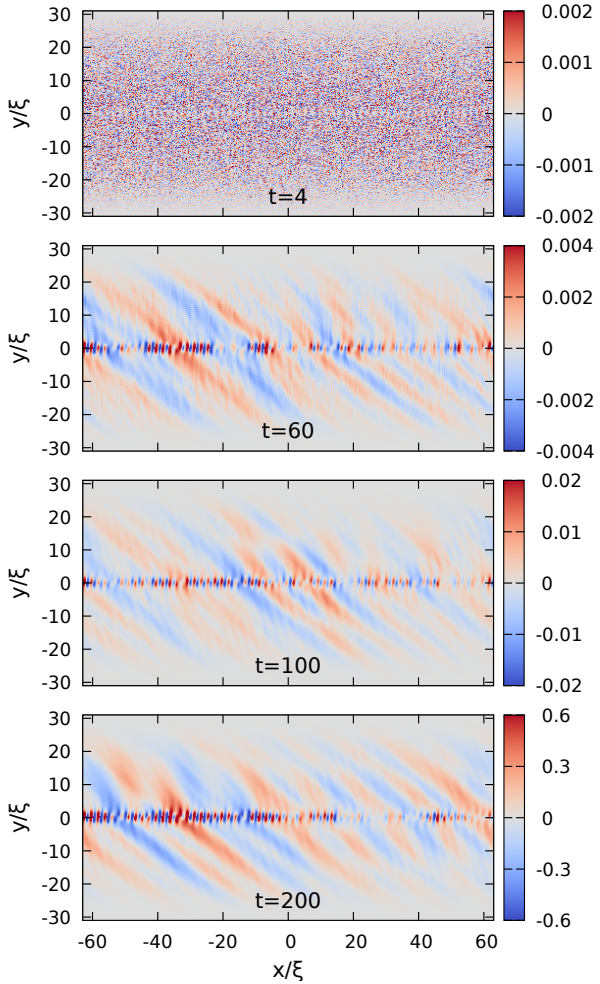


FIG. 6. Snapshots of the time evolution of the density variations obtained by evolving in time the Bogoliubov equations for  $\Delta v = 3c_s$  starting from a noisy configuration. Two Gaussian absorbing regions around  $\pm L_y/2$  are included to simulate an infinite system. The growing unstable modes is composed by waves travelling along the array of vortices and by outgoing sound waves. Times are expressed in units of  $\hbar/\mu$ .

simulate an open system in the  $y$  direction (and avoid SRI). The resulting time evolution of the density variations  $\delta n = 2\text{Re}(\Psi_v^*(U + V^*))$  is shown in Figure 6.

One can see that the system continues to be dynamically unstable since a particular density perturbation is selected from the initial noise and grows (exponentially) in time. This has a part peaked around the vortices and, in a video of the evolution, can be seen to be composed by waves travelling along the quantized shear layer. Together with these localized excitations also waves propagating away from the shear layer are present; notice the striped pattern here that differs from the interference one in the second row of Figure 1 since here waves propagating towards the shear layer are not present. The instability corresponds hence to a simultaneous creation of surface waves with sound waves that radiate away, hence the name RI.

A quantitative comparison with the results of the diagonalizations can be obtained by extracting the instability rates from the data of the time evolution. We performed the spatial Fourier transform so to obtain the time evolution in momentum space; we then extracted, at each time, the largest Fourier component at each  $K$ . We then fitted for each  $K$  the time dependence of these Fourier components with an exponential in time. The resulting growth rates are shown as red empty circles in the  $L_y = 120\xi$  panel of Figure 5, where the error bars are the uncertainty given by the finite length of  $T = 500\mu/\hbar$  of our simulation. One can see that there is a good agreement with the largest instability rates obtained for a finite but large system. This confirms the expectation that the dynamically unstable branch in the lower panel of Figure 5 remains in an infinite system, and is hence responsible for the RI.

Conceptually similar mechanisms have been predicted for incompressible fluids with density stratification, in which internal waves can have negative energy and interfacial gravity waves can exist. Some configurations displaying SRI and others displaying RI have been considered (see §4 in [12] for references and a discussion). Interestingly, the system under study in the present work naturally displays both in the context of compressible fluids.

Notice that, while the SRI does not rely on the quantized nature of the shear layer and can be expected to take place in generic compressible fluids, the RI crucially relies on the small scale structure for the existence of the interfacial waves. Moreover it is similar in nature to the *ergoregion instability* of multiply quantized vortices [14], in which the splitting in singly quantized vortices is driven by the simultaneous growth of a mode localized in the core and another one propagating away.

### C. Small velocities regime

Up to now we characterized the regimes of instability occurring above and below  $\Delta v = 2c_s$ . However, while decreasing the velocity, a deviation from the linear KHI decrease of the instability rate occurs for small velocities  $\Delta v \lesssim 0.8c_s$ , as can be seen in the upper panel of Figure 3. The modes responsible for this change of behaviour are already visible in the first case in Figure 2, where some points that deviate from the main KHI branch are visible at the edge of the Brillouin zone  $K = \frac{M}{\hbar}v$ .

These are modes whose instability rate is essentially independent on the relative velocity, as can be seen in Figure 7, where the imaginary part of the frequencies of the unstable mode are shown for smaller velocities than the ones in Figure 2. These instabilities hence do not depend on the spacing between the vortices. Differently, the KHI maximum at  $K = 0$  diminishes with the velocity, until its instability rate falls below the one of the modes on the edge of the Brillouin zone. From Figure 3 one can also see that, differently from the KHI that

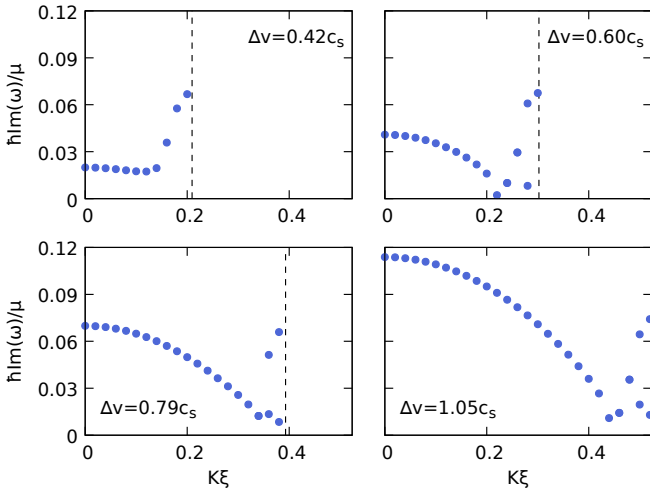


FIG. 7. Plots analogous to the ones of Figure 2, for  $L_y = 20\xi$ , but for small velocities. One can see, while lowering the velocity, the transition from the KHI regime of the last plot to a regime in which the instability is dominated by the modes near the edge of the Brillouin zone, that are essentially independent from the velocity.

is essentially independent on the system size, the dominating instability at small velocities is larger for smaller systems.

To get a better physical picture of these instabilities we performed time evolutions of the GPE, analogous to the ones of Figure 1, for small velocities differences and long times. While the long time fate of these evolutions is always of the KHI kind, with the vortices that displace from the central line and begin to corotate, at earlier times the behaviour is different.

This can be seen in Figure 8, where we show two snapshots of the density difference with respect to the state just after the complete formation of the quantized shear layer. Initially, density fluctuations grow equally around each vortex and correspond to a rigid displacement of the vortices along the central line. This is the effect of the fluctuations in the unstable modes on the edge of the Brillouin zone  $\delta\psi \propto e^{i\frac{M}{\hbar}vx}$ , that in fact correspond to density fluctuations  $\delta n = 2\text{Re}(\Psi^*\delta\psi) \sim \cos(2\frac{M}{\hbar}x)$ , with a periodicity equal to the distance between the vortices.

The origin of this displacement can be understood by performing numerical evolutions of the GPE with the vortex array placed at a different vertical position. What we observed (not shown) is that the direction of the horizontal motion depends on which is the nearest boundary. In the present case in which we consider a velocity directed to the left in the upper half and on the right in the lower half, we found that the vortices move to the right if placed nearer to the upper boundary and to the left if near the lower boundary.

This indicates that the rigid drift of the array has the same origin as the motion of a single vortex near a boundary of the condensate. This was studied in [20], where a

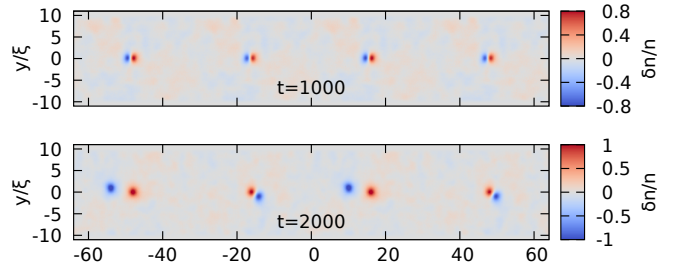


FIG. 8. Snapshots at long times of the evolution of the density fluctuations obtained by solving the GPE for  $\Delta v = 0.2 c_s$  and  $L_y = 20 \xi$ . The first snapshot at  $t = 1000 \mu/\hbar$  shows the result of the instability dominating at small velocities, while the second one at  $t = 2000 \mu/\hbar$  shows the subsequent development of a KHI.

semi-infinite condensate uniform condensate with a hard-wall boundary was considered. It was found that a vortex near this boundary moves parallel to it and that this motion can be understood by considering an *image vortex* with opposite circulation on the other side of the boundary, so that the motion of the vortex is analogous to a vortex-antivortex pair moving in parallel. This differs from the precession of vortices in an harmonic trap, that is mainly driven by the smooth density gradient towards the edge of the cloud. For a hard-wall instead the density reaches its bulk value within one healing length from the boundary and the effect of the density gradient is (exponentially) smaller.

In the present case we have two hard-wall boundaries, at equal distances from the vortices, so that the array can equally drift in both direction, along one of the image arrays of antivortices on the sides. One can hence think that the instability at small velocities stems from vertical fluctuations of the vortex array, that make it approach one of the two boundaries. The direction along which the array drifts will hence be given by the initial conditions in the fluctuations.

While being faster than the KHI for these velocities, this drift of the vortices does not prevent it from developing. This can be seen in the second snapshot of Figure 8, where the density fluctuations are clearly seen to change periodicity. The *hydrodynamic* instability of the shear layer hence continues to dominate also at small velocities, with the added physics of the lateral drift of vortices, that is obviously absent in the continuous hydrodynamic models.

## V. CONCLUSIONS

In this paper we investigated the stability properties of the quantized shear layer occurring at the interface between two counterpropagating flows in an atomic two-dimensional BEC and found a rich interplay between different instabilities. At relative velocities  $\Delta v < 2c_s$  we

found, as already predicted in [6], an instability analogous to the hydrodynamic KHI with the vortices displacing from their initial position and corotating. At small relative velocities, a lateral rigid drift of the vortices, analogous to the precession of vortices in a trapped condensate, occurs on time scales shorter than those of the KHI, that however continues to dominate the fate of the shear layer.

At higher relative velocities  $\Delta v > 2c_s$  instead, the KHI behaviour stops occurring due to the existence of phononic modes in which the modes responsible for the KHI can decay. However different instabilities emerge. In a small enough system along  $y$ , the instability is slower and develops with excitations accumulating in the two sides of the shear layer. This instability has its origin in the existence of negative energy modes in the system, associated to supersonic motion of the condensate, that can give rise to amplification, or superradiant scattering, of positive-energy excitation in the other half of the system (and the other way around). The repetition of this process gives rise to the SRI. If a larger (or infinite) system along  $y$  is considered, the SRI is replaced by the RI in which there is a simultaneous growth of interface waves travelling along the vortex array and of sound waves radiate away from it.

The mechanism responsible for SRI can be seen, through the ideas of analogue gravity, to be the same of superradiant instabilities in rotating spacetimes [10]. The occurrence of this kind of instability in the present system could be easily predicted from the point of view of our earlier work [13], in which a similar configuration (but

without vortices) was considered to gain insight into the physics of superradiant scattering. This work is hence an example in which analogies can help to look at problems from different perspectives.

While the suppression of the KHI and the SRI can be expected to occur in any compressible inviscid fluid, since they essentially rely on the properties of sound waves, the existence of the RI depends on the specific structure of the shear layer and on its possibility to support surface waves. It is also interesting to notice that the reliance of the RI on the resonance of localized excitations with propagating modes makes it similar in nature to the instabilities of multiply quantized vortices [14].

Even if in the present work we focused on atomic Bose-Einstein condensates, this physics can be expected to occur similarly in other systems such as quantum fluids of light [21], whose superfluid properties are under active study and whose controllability could also allow experimental investigations of the instabilities that we characterized here.

To conclude, we showed that the present setup displays an intriguing interplay between instabilities of different nature and with connections to various phenomena in different contexts, from well known behaviours of quantized vortices in trapped condensates, to classic hydrodynamic instabilities, to the physics of fields in curved spacetimes.

## ACKNOWLEDGEMENTS

We acknowledge financial support from the H2020-FETFLAG-2018-2020 project "PhoQuS" (n.820392) and from the Provincia Autonoma di Trento. L.G. thanks Giulia Piccitto for computational help.

---

- [1] F. Charru, *Hydrodynamic instabilities*, Vol. 37 (Cambridge University Press, 2011).
- [2] G. E. Volovik, On the Kelvin-Helmholtz instability in superfluids, *Journal of Experimental and Theoretical Physics Letters* **75**, 418 (2002).
- [3] R. Blaauwgeers, V. Eltsov, G. Eska, A. Finne, R. P. Hally, M. Krusius, J. Ruohio, L. Skrbek, and G. Volovik, Shear flow and Kelvin-Helmholtz instability in superfluids, *Physical review letters* **89**, 155301 (2002).
- [4] H. Takeuchi, N. Suzuki, K. Kasamatsu, H. Saito, and M. Tsubota, Quantum Kelvin-Helmholtz instability in phase-separated two-component Bose-Einstein condensates, *Physical Review B* **81**, 094517 (2010).
- [5] N. Suzuki, H. Takeuchi, K. Kasamatsu, M. Tsubota, and H. Saito, Crossover between Kelvin-Helmholtz and counter-superflow instabilities in two-component Bose-Einstein condensates, *Physical Review A* **82**, 063604 (2010).
- [6] A. Baggaley and N. Parker, Kelvin-Helmholtz instability in a single-component atomic superfluid, *Physical Review A* **97**, 053608 (2018).
- [7] L. D. Landau and E. M. Lifshitz, *Fluid mechanics. Fluid Mechanics. Second Edition.* 1987. Pergamon, Oxford (1987).
- [8] M. Karimi and S. S. Girimaji, Suppression mechanism of kelvin-helmholtz instability in compressible fluid flows, *Physical review E* **93**, 041102 (2016).
- [9] C. Barcelo, S. Liberati, and M. Visser, Analogue gravity, *Living reviews in relativity* **14**, 3 (2011).
- [10] R. Brito, V. Cardoso, and P. Pani, *Superradiance* (Springer, 2020).
- [11] T. Torres, S. Patrick, A. Coutant, M. Richartz, E. W. Tedford, and S. Weinfurtner, Rotational superradiant scattering in a vortex flow, *Nature Physics* **13**, 833 (2017).
- [12] A. D. Craik, *Wave interactions and fluid flows* (Cambridge University Press, 1988).
- [13] L. Giacomelli and I. Carusotto, Understanding superradiant phenomena with synthetic vector potentials in atomic Bose-Einstein condensates, *Physical Review A* **103**, 043309 (2021).
- [14] L. Giacomelli and I. Carusotto, Ergoregion instabilities in rotating two-dimensional Bose-Einstein condensates: Perspectives on the stability of quantized vortices, *Physical Review Research* **2**, 033139 (2020).
- [15] B. P. Anderson, P. Haljan, C. E. Wieman, and E. A. Cornell, Vortex precession in bose-einstein condensates: Observations with filled and empty cores, *Physical Re-*

view Letters **85**, 2857 (2000).

[16] L. Pitaevskii and S. Stringari, *Bose-Einstein condensation and superfluidity*, Vol. 164 (Oxford University Press, 2016).

[17] A. Michalke, On the inviscid instability of the hyperbolic tangent velocity profile, *Journal of Fluid Mechanics* **19**, 543 (1964).

[18] W. Blumen, Shear layer instability of an inviscid compressible fluid, *Journal of Fluid Mechanics* **40**, 769 (1970); W. Blumen, P. Drazin, and D. Billings, Shear layer instability of an inviscid compressible fluid. Part 2, *ibid.* **71**, 305 (1975); P. Drazin and A. Davey, Shear layer instability of an inviscid compressible fluid. part 3, *ibid.* **82**, 255 (1977).

[19] Y. Castin, Bose-Einstein condensates in atomic gases: simple theoretical results, in *Coherent atomic matter waves* (Springer, 2001) pp. 1–136.

[20] P. Mason, N. G. Berloff, and A. L. Fetter, Motion of a vortex line near the boundary of a semi-infinite uniform condensate, *Physical Review A* **74**, 043611 (2006).

[21] I. Carusotto and C. Ciuti, Quantum fluids of light, *Rev. Mod. Phys.* **85**, 299 (2013).